

## Three-dimensional eddy structure in a cylindrical container

By P. N. SHANKAR

CTFD Division, National Aerospace Laboratories, Bangalore 560017, India

(Received 12 March 1996 and in revised form 31 January 1997)

We consider Stokes flow in a cylindrical container of circular section induced by the uniform translatory motion of one of the endwalls. This flow field is of interest because it is possible to get reliable analytical descriptions of important three-dimensional structures such as the primary and corner eddies. It is shown, using a result of Tran-Cong & Blake, that separable solutions exist which can be combined to yield vector eigenfunctions that satisfy the sidewall boundary conditions provided the eigenvalues satisfy the transcendental equation

$$2kJ_2^2(k)J_0(k) - 6J_2(k)J_1(k)J_0(k) + kJ_1^2(k)\{J_0(k) - J_2(k)\} = 0.$$

The eigenstructure in the complex plane is somewhat unusual because the eigenvalues form two distinct sequences: a real-sequence  $\{\lambda_n\}$  and a complex sequence  $\{\mu_n\}$ , both of which need to be used to satisfy the top and bottom boundary conditions. The complex eigenvalue with the smallest real part, approximately  $2.568 + 1.123i$ , determines the spacing and decay of the intensity of the primary eddies in deep containers.

The above vector eigenfunctions are first combined, using a least-squares procedure, to determine the flow field in a container of infinite height. It is found, as in the corresponding two-dimensional case, that there is an infinite number of almost equally spaced counter-rotating primary eddies spaced about 2.8 container radii apart. For containers of finite height the number of primary eddies depends on the height of the container; computations show that for container heights of 1 and 2 (based on the radius) there is a single primary eddy while there are two and four respectively for heights of 4 and 10. More interestingly, the corner eddies in the plane of symmetry, rather than being made up of closed streamlines, consist of streamlines that connect the two foci at opposite corners in the plane of symmetry. Detailed three-dimensional streamline plots show that away from this plane the flow is almost entirely azimuthal in the corner, a result that would not be evident from two-dimensional results. Other interesting three-dimensional features of the eddy structure are also found.

Finally, the growth and merger of the corner eddy as the container height  $h$  is increased beyond 3 is studied carefully. Among a number of interesting features, it is found that at some stage streamlines cease to flow into the focus in the centreplane and start, rather, to stream out, resulting in a growing limit surface in the eddy. First, contact between the limit surfaces on opposite sides of the eddy in the symmetry plane, with local flow from one focus to the other, takes place ( $h \simeq 3.161$ ) before the eddy is fully developed. Full merger then takes place when  $h \simeq 3.235$  following which the merged eddy gives way to the second primary eddy. We find the corner eddy structure to be quite complicated during the merger process; three-dimensional streamline plots show intricate and rather beautiful patterns in the flow field.

---

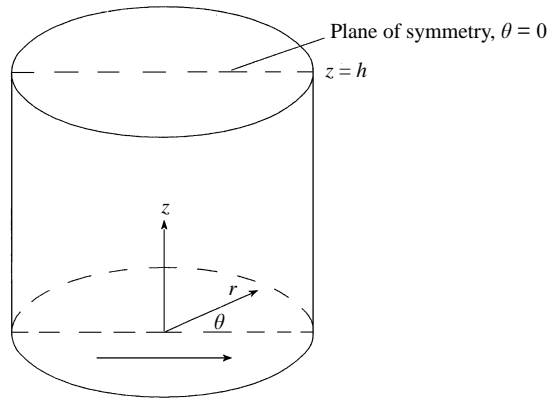


FIGURE 1. The geometry of the flow field considered.

## 1. Introduction

Although a very large number of papers have appeared and continue to appear on the two-dimensional flow in a cavity generated by the motion of one of the walls, very few have appeared on the corresponding three-dimensional problem. The few that have, for example Iwatsu *et al.* (1989), Verstappen & Veldman (1994), Zang, Street & Koseff (1994) and Deshpande & Shankar (1994), have invariably used direct computational methods to study these complex flow fields. While computational methods are powerful in their ability to handle complex geometries and the difficulties posed by nonlinearity, there are certain features of these flow fields that cannot, at present, be studied by these techniques. For example, the nature of the fields in deep cavities and the structure of delicate corner eddies cannot be examined by these methods. These require the use of analytical tools in a simple setting in order to be unambiguously resolved. The purpose of the present work is to study a three-dimensional recirculating flow in a convenient geometry with the aim of shedding light on certain canonical features of these flows.

We wish to analyse, with the above aim in mind, Stokes flow in a cylindrical container of circular section generated by the motion of one of the end plates of the container. The geometry is shown in figure 1, where the bottom of the container moves in the  $\theta = 0$  direction. If all velocities are normalized by the linear speed of the bottom wall, all lengths by  $R$ , the radius of the container, and the pressure suitably, the governing equations are

$$\nabla \cdot \mathbf{u} = 0, \quad \nabla p = \nabla^2 \mathbf{u},$$

The velocity  $\mathbf{u}$  has to vanish on the cylindrical sidewall of the container and on the top, and satisfy the no-slip condition on the bottom. Of particular interest are the primary eddies and their dependence on the non-dimensional height  $h$  of the container, and the structure of the corner eddies located near the top corner of the container. We will show that this simple-looking flow field is rich in fluid mechanical detail.

## 2. Analysis

We wish to analyse the flow field in the container using an eigenfunction expansion. It proves to be convenient to use a general result of Tran-Cong & Blake (1982). They show that if  $\mathbf{B}$  and  $B_0$  are vector and scalar fields satisfying Laplace's equation, i.e.  $\nabla^2 \mathbf{B} = 0$  and  $\nabla^2 B_0 = 0$ , then the velocity field

$$\mathbf{v} = \nabla(\mathbf{r} \cdot \mathbf{B} + B_0) - 2\mathbf{B} \quad (1)$$

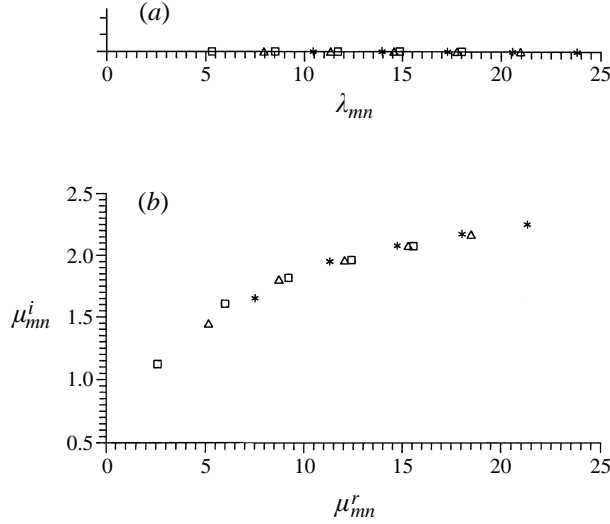


FIGURE 2. The first five eigenvalues for  $m = 1, 3$  and  $5$ : (a) the real eigenvalues and (b) the complex ones.  $\square$ ,  $m = 1$ ;  $\triangle$ ,  $m = 3$ ;  $*$ ,  $m = 5$ .

will be solenoidal and satisfy Stokes' equation. Since separable solutions to the scalar Laplace equation are easily obtained, we need only to find solutions to the vector Laplace equation in cylindrical coordinates.

For the flow field in the geometry considered here, it is natural to look for separable solutions of the form  $f(r)e^{im\theta+ksz}$ . For the required scalar field  $B_0$ ,  $f(r)$  is simply  $J_m(kr)$ . We then need two vector fields  $\mathbf{B}_1$  and  $\mathbf{B}_2$  which satisfy the vector Laplace equation. Using the results given in Morse & Feshbach (1953, p. 1797) one can write down the following forms for the vector fields:

$$\mathbf{B}_1 = e^{kz} \left[ \mathbf{a}_r \begin{pmatrix} -\sin m\theta \\ \cos m\theta \end{pmatrix} \{J_{m-1}(kr) + J_{m+1}(kr)\} - \mathbf{a}_\theta \begin{pmatrix} \cos m\theta \\ \sin m\theta \end{pmatrix} \{J_{m-1}(kr) - J_{m+1}(kr)\} \right], \quad (2a)$$

$$\mathbf{B}_2 = e^{kz} \left[ \mathbf{a}_r \begin{pmatrix} \cos m\theta \\ \sin m\theta \end{pmatrix} \{J_{m-1}(kr) - J_{m+1}(kr)\} + \mathbf{a}_\theta \begin{pmatrix} -\sin m\theta \\ \cos m\theta \end{pmatrix} \{J_{m-1}(kr) + J_{m+1}(kr)\} \right]. \quad (2b)$$

It will be convenient now to make use of the fact that, when the flow is driven by the uniform movement of the bottom wall in the  $\theta = 0$  direction, the field will be symmetrical about the plane  $\theta = 0$ . Doing this, if we now utilize the fields  $\mathbf{B}_0$ ,  $\mathbf{B}_1$  and  $\mathbf{B}_2$  in the ratios  $1:b:c$ , formula (1) yields a candidate velocity field whose components are given by

$$v_r(r, \theta, z) = e^{kz} \cos m\theta [J'_m + b\{(m-2)J_{m-1} - (m+2)J_{m+1}\} + c\{(-2krJ_m + (m-2)J_{m-1} + (m+2)J_{m+1}\}], \quad (3a)$$

$$v_\theta(r, \theta, z) = e^{kz} \sin m\theta [-mJ_m/r + b\{(2-m)J_{m-1} - (2+m)J_{m+1}\} + c\{(2-m)J_{m-1} + (2+m)J_{m+1}\}], \quad (3b)$$

$$v_z(r, \theta, z) = e^{kz} \cos m\theta [J_m + rb\{J_{m-1} + J_{m+1}\} + rc\{J_{m-1} - J_{m+1}\}]. \quad (3c)$$

In order to save space, the argument of the Bessel functions,  $kr$ , has been dropped in the above equations.

The boundary conditions require that all the three components of the velocity vanish

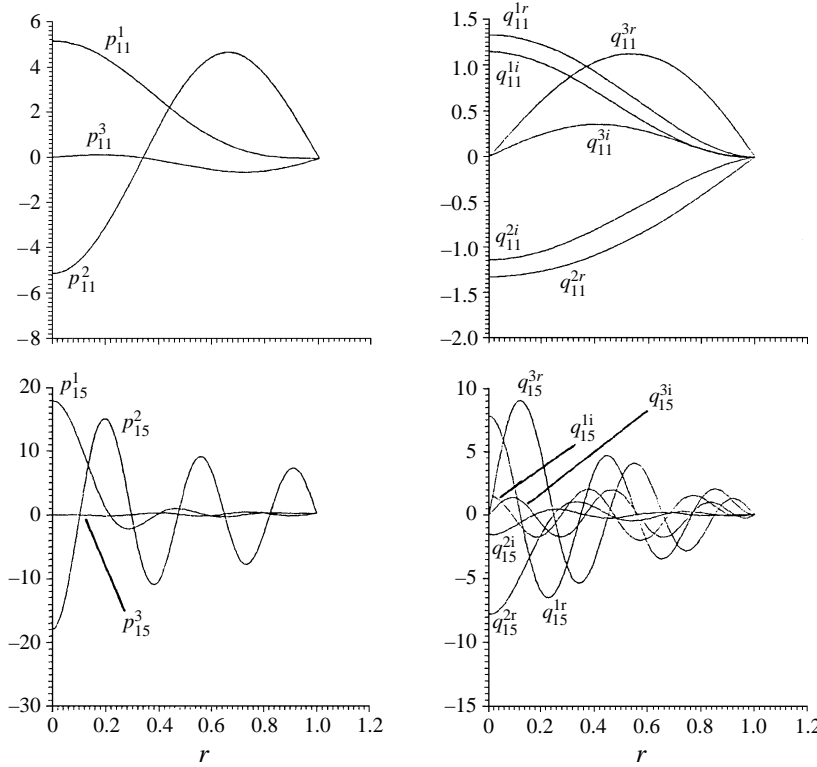


FIGURE 3. The shapes of the components of the vector eigenfunctions  $p_{mn}(r)$  and  $q_{mn}(r)$  for  $m = 1$  and  $n = 1$  and  $5$ .

$n$	$\lambda_{1n}$	$\mu_{1n}$
1	5.317	$2.568 + 1.123i$
2	8.533	$6.004 + 1.608i$
3	11.70	$9.232 + 1.817i$
4	14.86	$12.42 + 1.961i$
5	18.02	$15.59 + 2.073i$
6	21.16	$18.75 + 2.163i$
7	24.31	$21.90 + 2.240i$
8	27.46	$25.05 + 2.307i$
9	30.60	$28.20 + 2.366i$
10	33.75	$31.35 + 2.418i$

TABLE 1. The first ten real and complex eigenvalues  $\lambda_{1n}$  and  $\mu_{1n}$

on  $r = 1$ . This requirement leads to an eigenvalue problem for the exponent  $k$ . It is easy to show that  $k$  has to satisfy the transcendental equation

$$2kJ_{m+1}^2(k)J_{m-1}(k) - 2(m+2)J_{m+1}(k)J_m(k)J_{m-1}(k) + kJ_m^2(k)\{J_{m-1}(k) - J_{m+1}(k)\} = 0. \tag{4}$$

If  $k^*$  satisfies (4) the components given in (3) yield a vector eigenfunction provided the constants  $b$  and  $c$  take the values

$$b = -\frac{J_m(k^*)\{J_{m-1}(k^*) + J_{m+1}(k^*)\}}{4J_{m-1}(k^*)J_{m+1}(k^*)}, \quad c = -\frac{\{J_{m-1}(k^*) - J_{m+1}(k^*)\}b}{J_{m-1}(k^*) + J_{m+1}(k^*)}. \tag{5}$$

To the best of our knowledge the equation determining the eigenvalues, equation (4), does not seem to have appeared in the fluid mechanical literature before. However, a referee has pointed out that Dougall (1913) derived a similar equation when considering the equilibrium of an elastic rod of circular section. Based on what is known from the two-dimensional cavity problem, we expect to find infinite sequences of complex eigenvalues for each  $m$ ; for deep cavities then the eddy structure would be determined by the eigenvalue with the smallest real part. What we actually find is a little more complicated: for each  $m$  there exists not only a complex sequence  $\{\mu_{mn}\}$  of eigenvalues but also a real sequence  $\{\lambda_{mn}\}$ . This is illustrated in figure 2, which shows the first five in each sequence, in the right half-plane, for  $m = 1, 3$  and  $5$ . For each  $m$ , succeeding eigenvalues after the first shift to the right while the imaginary part increases slightly for the complex sequences; with increasing  $m$ , the first eigenvalues of the sequences,  $\lambda_{m1}$  and  $\mu_{m1}$ , shift to the right. For each  $m$  the difference between the real parts of consecutive eigenvalues, i.e.  $(\mu_{mn+1}^r - \mu_{mn}^r)$  and  $(\lambda_{mn+1} - \lambda_{mn})$ , decreases and seems to tend to  $\pi$  as  $n \rightarrow \infty$ .

The actual computation of the eigenvalues was done using Newton's method. As in all cases involving complex roots, the principle of the argument has to be used to ensure that all the roots in a given part of the complex plane have been found. Table 1 lists the first ten real and complex eigenvalues for  $m = 1$  correct to four significant figures only for clarity. In the computation of the field, roots correct to at least 12 digits were used (Shankar 1996 gives detailed tables of the eigenvalues). The 1st and 5th eigenfunctions for the  $m = 1$  case are displayed in figure 3. As one would expect, as  $n$  increases the functions increasingly oscillate between 0 and 1.

In order to be able to use these eigenfunctions in an expansion procedure for our problem it is important that certain symmetries exist. It is easy to show from (4) that if  $\lambda$  and  $\mu$  are eigenvalues, then so are  $-\lambda$ ,  $-\mu$  and  $\bar{\mu}$ . Thus there is the possibility of expanding real functions in terms of these and of handling both the top and bottom boundary conditions.

Let

$$\mathbf{p}_{mn}(r) = (p_{mn}^1(r), p_{mn}^2(r), p_{mn}^3(r)) \quad \text{and} \quad \mathbf{q}_{mn}(r) = (q_{mn}^1(r), q_{mn}^2(r), q_{mn}^3(r))$$

be the vector eigenfunctions corresponding to  $\lambda_{mn}$  and  $\mu_{mn}$  respectively. Then, in general, we can attempt to expand the velocity field  $\mathbf{u}(r, \theta, z)$  in the following manner:

$$u_r = \sum_m \sum_n \cos m\theta \{ [a_{mn} e^{-\lambda_{mn}z} + c_{mn} e^{-(h-z)\lambda_{mn}}] p_{mn}^1(r) + \text{Re} \{ [b_{mn} e^{-\mu_{mn}z} + d_{mn} e^{-(h-z)\mu_{mn}}] q_{mn}^1(r) \} \}, \quad (6a)$$

$$u_\theta = \sum_m \sum_n \sin m\theta \{ [a_{mn} e^{-\lambda_{mn}z} + c_{mn} e^{-(h-z)\lambda_{mn}}] p_{mn}^2(r) + \text{Re} \{ [b_{mn} e^{-\mu_{mn}z} + d_{mn} e^{-(h-z)\mu_{mn}}] q_{mn}^2(r) \} \}, \quad (6b)$$

$$u_z = \sum_m \sum_n \cos m\theta \{ [-a_{mn} e^{-\lambda_{mn}z} + c_{mn} e^{-(h-z)\lambda_{mn}}] p_{mn}^3(r) + \text{Re} \{ [-b_{mn} e^{-\mu_{mn}z} + d_{mn} e^{-(h-z)\mu_{mn}}] q_{mn}^3(r) \} \}. \quad (6c)$$

It may be noted that eigenvalues from both halves of the complex plane are used; further that the negative signs in (6c) are needed because the changes  $\lambda \rightarrow -\lambda$  and  $\mu \rightarrow -\mu$  require that  $(p^1, p^2, p^3) \rightarrow (p^1, p^2, -p^3)$  and  $(q^1, q^2, q^3) \rightarrow (q^1, q^2, -q^3)$  respectively.

Considerable simplification can now be achieved by qualitative use of the boundary conditions. Whereas  $\mathbf{u} = \mathbf{0}$  at  $z = h$ , at  $z = 0$  we require  $\mathbf{u}$  to equal  $\mathbf{U}_0 = (\cos \theta, -\sin \theta, 0)$ . Now the orthogonality of the trigonometric functions implies that  $a_{mn} = b_{mn} = c_{mn} = d_{mn} = 0$  if  $m \neq 1$ , i.e. we need  $m = 1$  alone for these boundary

conditions. Thus only the terms involving the first harmonic in  $\theta$  need be retained. In all of the following the first subscript will be dropped with the understanding that  $m = 1$ . The velocity field then has the representation

$$\mathbf{u} = \sum_n \left[ a_n \begin{pmatrix} \cos \theta p_n^1 \\ \sin \theta p_n^2 \\ -\cos \theta p_n^3 \end{pmatrix} e^{-\lambda_n z} + c_n \begin{pmatrix} \cos \theta p_n^1 \\ \sin \theta p_n^2 \\ \cos \theta p_n^3 \end{pmatrix} e^{-(h-z)\lambda_n} \right. \\ \left. + \text{Re} \left\{ b_n \begin{pmatrix} \cos \theta q_n^1 \\ \sin \theta q_n^2 \\ -\cos \theta q_n^3 \end{pmatrix} e^{-\mu_n z} + d_n \begin{pmatrix} \cos \theta q_n^1 \\ \sin \theta q_n^2 \\ \cos \theta q_n^3 \end{pmatrix} e^{-(h-z)\mu_n} \right\} \right]. \quad (7)$$

The coefficients  $a_n$ ,  $b_n$ ,  $c_n$  and  $d_n$  are now determined, as in the two-dimensional case (Shankar 1993), by a least-squares procedure. Taking  $N$  terms in the sum in (7) and  $I$  points on  $(0, 1)$ , let  $e_1^2, e_2^2, \dots, e_6^2$  be the sums of the total errors squared in the satisfaction of the six boundary conditions at the chosen  $I$  points. Then consider  $E_T^2 = e_1^2 + e_2^2 + \dots + e_6^2$ . The  $6N$  real constants to be found can now be determined by solving the  $6N$  linear equations resulting from the minimization of  $E_T^2$  with respect to the coefficients. Computations using  $N = 10, 20, 40$  and  $60$  showed that the coefficients converge rapidly.

A technical point to be noted, though minor from a practical point of view, is that the boundary conditions on  $u_r$  and  $u_\theta$  change discontinuously at  $r = 1$  at the bottom of the container. For the two-dimensional case this discontinuity has been found not to significantly affect the field away from the singular edges (Srinivasan 1995). We have assumed that this holds in the present case too; however, in the minimization procedure we have ensured that the last minimization point is  $\epsilon$  ( $\epsilon \neq 0$ ) away from  $r = 1$ . Thus the minimization points are equally spaced from  $(1 - \epsilon)/I$  to  $1 - \epsilon$ . There is no unique value for  $I$ ; for all the calculations reported here  $I = 3N$  with  $N = 100$  and  $\epsilon = 0.02$ .

Before discussing the results some indication will now be given of the order of magnitude of the errors made in the satisfaction of the boundary conditions at the bottom and top of the container. These errors will naturally be largest near  $r = 1$  where the discontinuities occur and so we shall concentrate our attention on this neighbourhood. The three components of velocity at  $z = 0$  and  $z = 1$ , the top for a container of unit height, are shown in figure 4 on the interval  $0.85 < r < 0.99$  with a change of scale at  $r = 0.95$  in order to accommodate the larger errors near  $r = 1$ . On  $z = 0$  the errors in  $u_r$  begin to build up earliest around  $r = 0.9$ , being oscillatory initially, but around  $r = 0.98$  both  $u_r$  and  $u_\theta$  monotonically decay to their boundary value of zero. On the other hand the error in  $u_z$  builds up much later, around  $0.985$ , before decaying to the boundary value. On the top wall the errors are of the order of  $10^{-8}$  or better until  $r = 0.98$  guaranteeing that the corner eddies will be captured accurately. It should be pointed out that in figure 4 the errors are shown at non-minimization points, i.e. where the errors will, generally, be larger, and also that the errors are actually smaller for larger container heights.

It may be mentioned here that two types of procedures were employed to make sure that the computations were, mathematical questions of convergence and completeness apart, as reliable and accurate as possible. First,  $N$  was increased from 60 to as much as 500 in special cases to check that the expansion coefficients were 'converging' and to check that the major features of the field were unaffected by increasing  $N$ . Secondly, to make sure that round-off was not a problem at high  $N$ , quadruple-precision

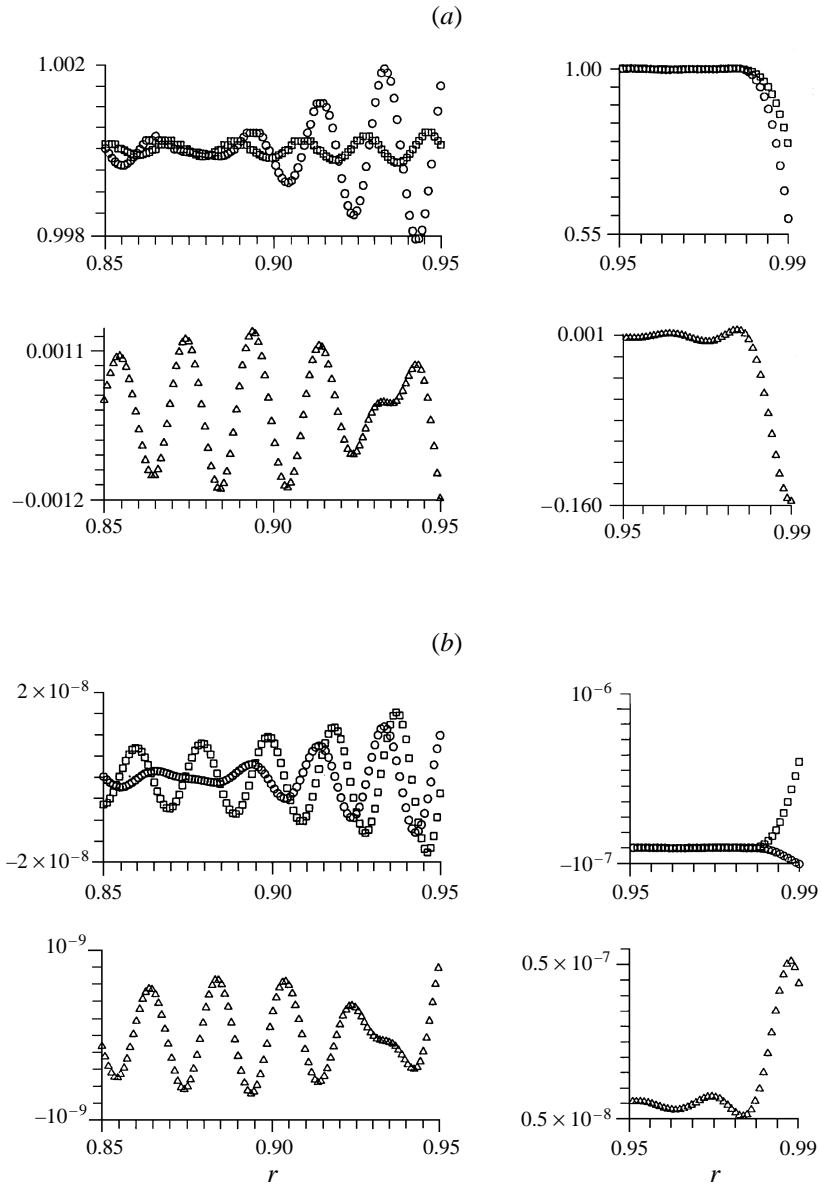


FIGURE 4. The behaviour of the computed velocity components in the neighbourhood of  $r = 1$  at (a) the bottom and (b) top walls.  $h = 1$ ,  $N = 100$ ,  $I = 300$  and  $\epsilon = 0.02$ .  $\circ$ ,  $u_r$ ;  $\square$ ,  $u_\theta$ ;  $\triangle$ ,  $u_z$ .

arithmetic was employed in special cases as a check. No inconsistencies or ambiguities were detected. We observe that in order to resolve the corner eddies to increasing detail,  $N$  has to be increased (and  $\epsilon$  decreased) so that the top boundary conditions, especially near the corner, are satisfied to sufficient accuracy.

### 3. The field in a container of infinite height

We begin, in order to simplify matters, by considering a container of infinite height, i.e.  $h = \infty$ . In the corresponding two-dimensional case (Shankar 1993) it is known that the flow field consists of an infinite number of almost equally spaced counter-rotating

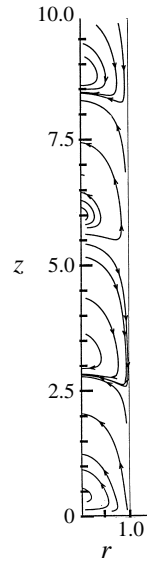


FIGURE 5. The eddy structure in a container of infinite height. Streamlines in one half of the plane of symmetry  $\theta = 0$  are shown.

$n$	$a_n$	$b_n$
1	-0.1308	$-0.2980 - 0.1122 \times 10i$
2	$0.6063 \times 10^{-1}$	$0.5842 \times 10^{-1} + 0.4046i$
3	$-0.3621 \times 10^{-1}$	$-0.9828 \times 10^{-2} - 0.2652i$
4	$0.2458 \times 10^{-1}$	$-0.4346 \times 10^{-2} + 0.1974i$
5	$-0.1803 \times 10^{-1}$	$0.9485 \times 10^{-2} - 0.1570i$
6	$0.1391 \times 10^{-1}$	$-0.1147 \times 10^{-1} + 0.1302i$
7	$-0.1114 \times 10^{-1}$	$0.1218 \times 10^{-1} - 0.1112i$
8	$0.9159 \times 10^{-2}$	$-0.1232 \times 10^{-1} + 0.9691 \times 10^{-1}i$
9	$-0.7691 \times 10^{-2}$	$0.1221 \times 10^{-1} - 0.8584 \times 10^{-1}i$
10	$0.6566 \times 10^{-2}$	$-0.1199 \times 10^{-1} + 0.7699 \times 10^{-1}i$

TABLE 2. The first ten coefficient  $a_1, b_1, \dots, a_{10}, b_{10}$  for the cavity of infinite depth

eddies. The fact that a sequence of complex eigenvalues  $\{\mu_n\}$  exists in the present case suggests that the situation will be similar here. It is required now to drop the terms involving the eigenvalues with positive real part in (7) and so the simpler representation

$$\mathbf{u} = \sum_n \left[ a_n \begin{pmatrix} \cos \theta p_n^1 \\ \sin \theta p_n^2 \\ -\cos \theta p_n^3 \end{pmatrix} e^{-\lambda_n z} + \text{Re} \left\{ b_n \begin{pmatrix} \cos \theta q_n^1 \\ \sin \theta q_n^2 \\ -\cos \theta q_n^3 \end{pmatrix} e^{-\mu_n z} \right\} \right] \quad (8)$$

is sufficient. Thus if  $N$  terms are retained only  $3N$  real constants need to be solved for.

The first ten coefficients for this case are listed in table 2; although all computations have been carried out using double-precision arithmetic and are correct to a much larger number of places, only the first few significant digits are listed here for clarity. It may be noted from this table that, as in the two-dimensional case, the coefficients decay slowly and alternate in sign. Surprisingly, however, just 20 terms usually suffice to give a good picture of the flow field; this is because as  $z$  increases the first few eigenvalues, with smaller real part, dominate.



$h$	1st	2nd	3rd	4th	5th
1	0.3121	—	—	—	—
2	0.3999	—	—	—	—
4	0.4012	3.1653	—	—	—
10	0.4012	3.1992	5.9977	8.7888	—
$\infty$	0.4012	3.1992	5.9977	8.7961	11.5946

TABLE 3. The locations of the centres of the primary eddies in the plane  $\theta = 0$  for various cylinder heights. The numbers indicate the  $z$  coordinate

The streamlines in the plane of symmetry  $\theta = 0$  are shown in figure 5. As expected from the nature of the eigenvalues and by analogy with the two-dimensional situation, the flow field consists of an infinite sequence of counter-rotating eddies. Although this is generally not true in three dimensions, the streamlines are closed curves; this is a consequence of the fact that for Stokes flow the field has to be symmetric about the  $\theta = \pi/2$  plane. Although one cannot tell from the symmetry-plane picture alone, it appears that the eddies are separate and distinct. This will be discussed in more detail later.

The approximate locations of the eddy centres in the symmetry plane are listed in table 3. It may be noted that the spacing between successive centres settles to a value of about 2.799. Referring to table 1, the imaginary part of the dominant eigenvalue is about 1.1226; this would imply a spacing of about  $\pi/1.1226 \simeq 2.798$ , in agreement with what is found.

The three-dimensional nature of the eddies away from the symmetry plane will be discussed later when we deal with containers of finite height.

#### 4. The overall eddy structure in containers of finite height

When  $h$  is finite all  $6N$  real coefficients have to be solved for as the exponents with positive real part have now to be retained. As may be expected, it is found that as  $h$  increases  $c_n$  and  $d_n$  decrease while  $a_n$  and  $b_n$  tend to the values given in table 2 for the  $h = \infty$  case.

The streamline patterns in the symmetry plane  $\theta = 0$  are shown in figure 6. For both the cases  $h = 1$  and  $h = 2$  the primary flow consists of a single recirculating eddy; there are two counter-rotating primary eddies when  $h = 4$  and four primary eddies when  $h = 10$ . The corner eddies can be seen for the two shorter containers; they also exist for the other two cases also but are not resolved with the coarse grid used to generate these pictures. The locations of the centres of the primary eddies in the plane  $\theta = 0$  are listed in table 3. Note that the spacing quickly settles to its asymptotic value of about 2.8.

The nature of the corner eddy in the plane  $\theta = 0$  can be better understood from figure 7(a) which shows the corner region for  $h = 2$ . Unlike the situation in the two-dimensional case where the eddy is made up of closed streamlines, the streamlines forming the corner eddy here come from the other corner in the same plane at  $\theta = \pi$ ; this can be seen from figure 7(b). The streamlines converge to and meet at a focus, which we shall call the centre of the corner eddy in the symmetry plane; this is a typically three-dimensional feature in the flow field. The eddy centre is a stagnation point and one would expect the flow to be azimuthal in this neighbourhood in nearby adjacent planes. A matter of some interest is the nature of the ‘separation streamline’ in the plane of symmetry. Figure 7(b) shows the separation streamline  $s_1$  and two

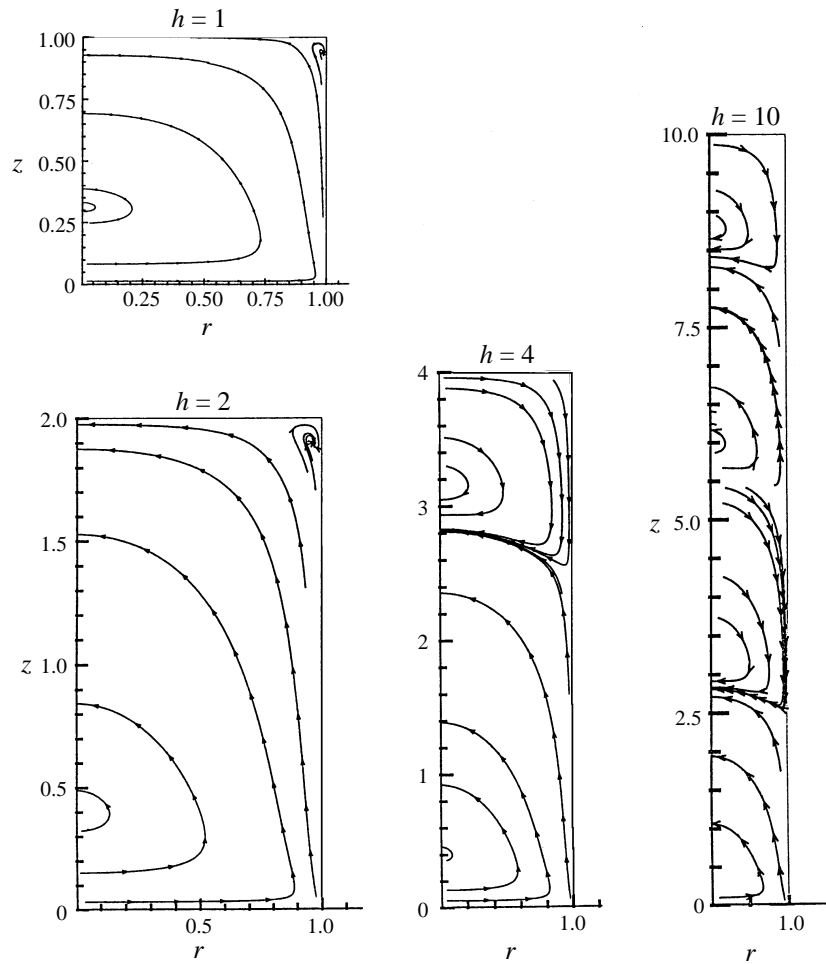


FIGURE 6. Streamlines in the plane  $\theta = 0$  for containers of height 1, 2, 4 and 10. Only a half of the symmetry plane is shown in each case.

nearby streamlines,  $s_2$  which is part of the primary eddy and  $s_3$  which is part of the corner eddy. As figures 7(a) and 7(b) show, the separation streamline starts from a point about 0.2 away from the cylindrical sidewall on the plane  $z = h$  at  $\theta = \pi$ , moves down the container, turns near the bottom, moves to the centreline and then traces a symmetrical path to the top of the container. The 'corner eddy', which lies between this and the container surface, thus occupies a significant portion of the container even far from the corner. This is totally different from the analogous two-dimensional field where the corner eddy is actually confined to the corner! The locations of the (first) corner eddy centres and the widths of these eddies along the top of the container in the plane  $\theta = 0$  for various cavity heights are given in table 4. An interesting question that comes to mind is whether, as in the two-dimensional case (Moffatt 1964), the corner eddies form an infinite sequence of decreasing size and intensity. This question will be discussed a little later.

For a complex three-dimensional flow, even for one with as much symmetry as the one considered here, three-dimensional streamline plots are essential to get a complete picture of the field. Since the flow is steady, streamlines can be found by releasing

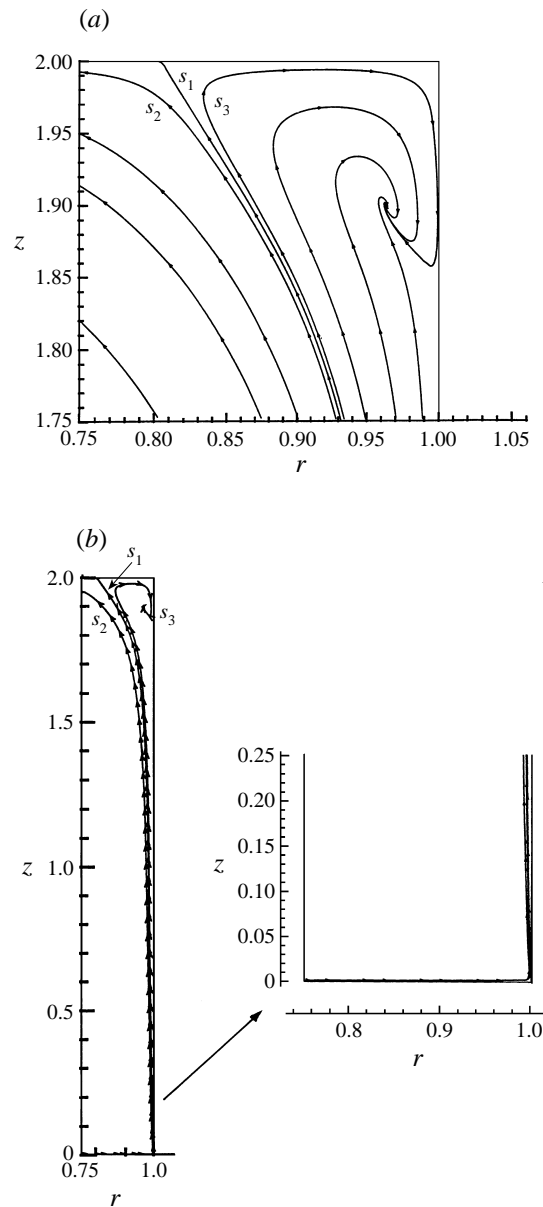


FIGURE 7. (a) A close-up of the corner eddy in the symmetry plane  $\theta = 0$ , showing the separation streamline  $s_1$ . (b) The separation streamline and two nearby streamlines in the plane  $\theta = 0$ . The inset shows that the streamlines that make up the corner eddy connect the two foci.  $h = 2$ .

imaginary tracer particles in the field and tracking their paths by integrating the equations of motion. The streamlines displayed here were obtained using a commercial software package called CFD-VIEW with the computed velocity field as input. Two views of the same three-dimensional streamlines are shown in figure 8 for a container of height 2. Streamlines  $s_1$  and  $s_2$  loop around the curved line (not shown) that forms the centreline or stagnation line of the primary eddy. This line is located in the plane  $\theta = \pi/2$ . Next consider the streamline  $s_3$ , which it should be made clear nowhere intersects the plane  $\theta = 0$ . It starts near the bottom, i.e. near the moving end plate, in

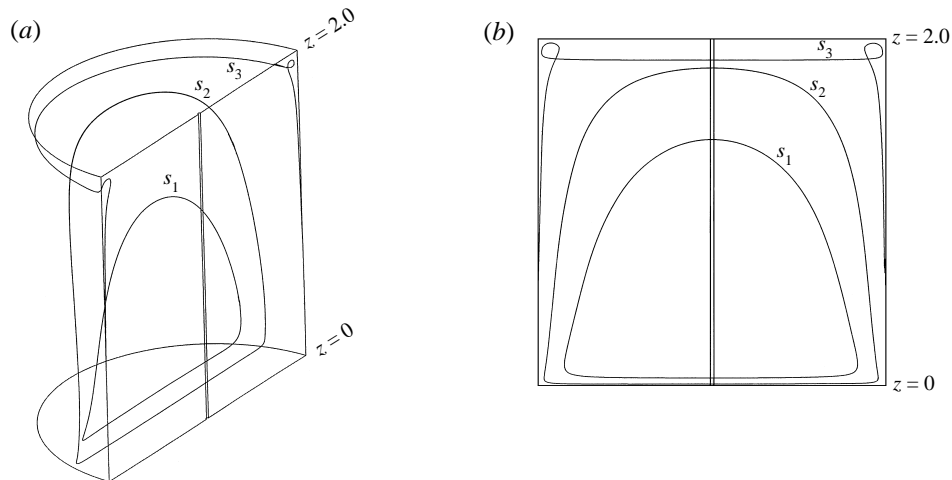


FIGURE 8. Two views of three-dimensional streamlines in a container of height 2.

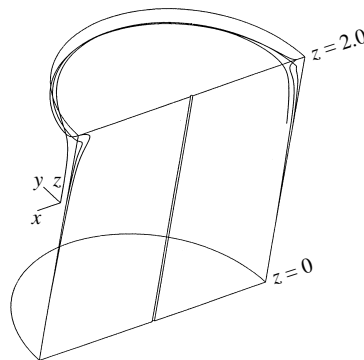


FIGURE 9. Three streamlines that contribute to the primarily azimuthal flow in the corner eddy away from the symmetry plane.  $h = 2$ .

---

$h$	Location $(r, z)$	Width
1	(0.984, 0.938)	0.116
2	(0.964, 1.900)	0.197
4	(0.983, 3.926)	0.138
10	(0.975, 9.913)	0.169

---

TABLE 4. The location of the centre and the width of the corner eddy at the top in the plane  $\theta = 0$

a plane slightly away from the symmetry plane, moves upwards into the corner eddy, makes a single loop, then moves azimuthally until it reaches the neighbourhood of  $\theta = \pi$ , makes another loop and goes back down to the neighbourhood of the moving plate before following an almost straight trajectory back to the starting point. The almost purely azimuthal motion, which can best be seen in figure 8(b), is somewhat surprising; based on what is known of two-dimensional corner eddies, one might have expected the streamline to show some spiralling motion. It now appears that away from the plane  $\theta = 0$  the motion in the corner eddy is almost purely azimuthal with

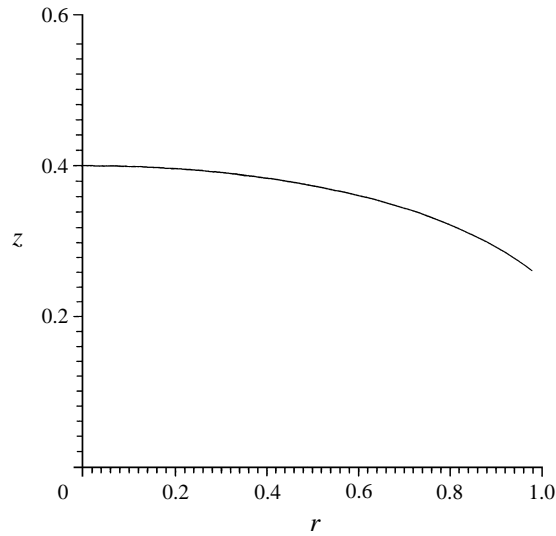


FIGURE 10. The centreline of the primary eddy in the plane  $\theta = \pi/2$ .  $h = 2$ .

fluid being fed from near the bottom of the container. This conclusion is strengthened by the streamlines shown in figure 9. Since the primary eddy is three-dimensional, we would expect its ‘centreline’, in the plane  $\theta = \pi/2$ , to be curved. We define the eddy centre in this plane to be the location where  $u_\theta$  vanishes. Figure 10 shows the curved centreline of the primary eddy: whereas the centre is about 0.4 above the bottom at  $r = 0$ , it is only 0.26 above the bottom at the cylindrical wall. The curvature is somewhat more than might have been expected.

A remark is appropriate now on a common feature of the streamlines in these flows. One cannot in general expect streamlines to be closed in three-dimensional flows. However, the Stokes flows considered here demand symmetry about the plane  $\theta = \pi/2$ . Now streamlines which cut this plane twice have, by this symmetry, to be closed. Thus all streamlines originating away from the plane  $\theta = 0$  are closed including ones that make up the corner eddy. In the symmetry plane  $\theta = 0$ , however, only the streamlines that make up the primary eddy are closed. The other streamlines start from one focus in the corner eddy and end up, in a symmetrical manner about  $\theta = \pi/2$ , at the other focus. It may be recalled that in two dimensions the corner eddies are made up of closed streamlines and are separated from the primary eddy by separation streamlines. The corner eddies here are quite different both in the symmetry plane and away from it where the azimuthal flow dominates.

Finally, we examine the nature of the interface between two primary eddies. Figure 11 shows three-dimensional streamline plots near such an interface for a container of height 4. In this figure streamlines  $s_1$  and  $s_2$  are in the first primary eddy while  $s_3$ – $s_6$  are all in the second primary eddy. The latter streamlines clearly show the eddying motion in the second primary eddy. Streamlines  $s_5$  and  $s_6$  approach  $s_1$  and  $s_2$  near the interface as they lie in the same plane in that neighbourhood; whereas  $s_3$  lies entirely in the second primary eddy,  $s_6$  takes part in the azimuthal motion near the top of the container. Streamline plots such as this and others give strong support to the view that the primary eddies are separated from one another by separation surfaces. However no formal proof exists for this view.

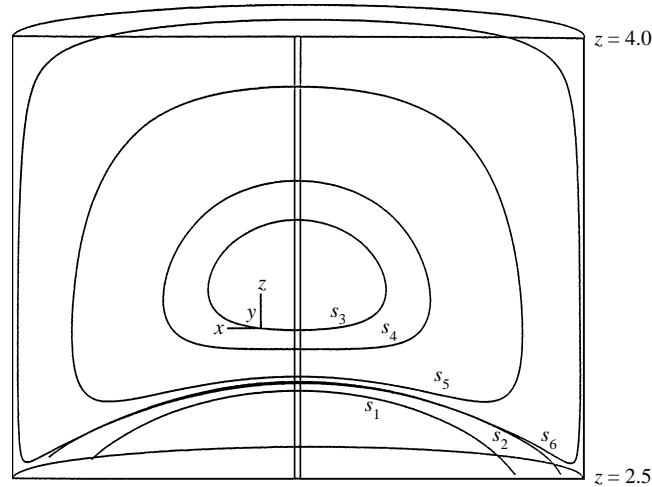


FIGURE 11. Three-dimensional streamline plots showing the second primary eddy and the boundary between it and the primary eddy.  $h = 4$ .

### 5. Corner eddy merger and the evolution of the primary eddies

It is known from the considerable work done on the two-dimensional version of this problem that, in two dimensions, there is an infinite sequence of eddies of decreasing strength and size near each of the fixed corners (Moffatt 1964); moreover, that near certain critical values of container height the primary corner eddies rather suddenly increase in size with height and ultimately merge to generate a new primary eddy (Shankar 1993). A natural question now is: what happens in this three-dimensional geometry? Although we do not have, as yet, an equivalent to Moffatt's result in three dimensions, careful computations show that higher-order corner eddies do exist in this geometry too. For example, figure 12 shows the centreplane flow field in a container of height 3, most of which consists of a single primary eddy made up entirely of closed streamlines. The corner eddies, the details of which are shown in parts (b) and (c), are made up of streamlines that spiral into and out of foci. As pointed out earlier, the streamlines that make up the first corner eddy in the plane  $\theta = 0$  connect the two foci on either side of the plane  $\theta = \pi/2$ . In this particular case, since the first corner eddy is already quite large, the second corner eddy, shown in figure 12(c), can be resolved with just 100 eigenfunctions and accurately plotted with double the number and with  $\epsilon = 0.01$ . On the other hand, when  $h = 2$  the primary corner eddy is still small and so the second corner eddy is only poorly resolved with 200 eigenfunctions. For the streamlines shown in figure 13(a), 500 eigenfunctions were used with  $\epsilon = 0.004$ . Another point of interest is that whereas the streamlines diverge from the focus of the second corner eddy for  $h = 3$  and  $h = 3.235$  (shown in figure 13b), the streamlines converge to the focus in the case  $h = 2$ .

In the two-dimensional cavity case, it was shown that around a critical depth of about 1.62 cavity widths the corner eddies suddenly increased in size as the depth was increased. This led to the merger of the first corner eddies; the merger then resulted in the formation of the second primary eddy. In the three-dimensional geometry considered here, it is known that for  $h = 3$  there is only one primary eddy while there are two for  $h = 4$ . We may therefore, in analogy with the two-dimensional case, expect the first corner eddy to grow rapidly and merge around some height in the range  $3 < h < 4$ . This question will be examined now. Figure 14 shows the evolution of the

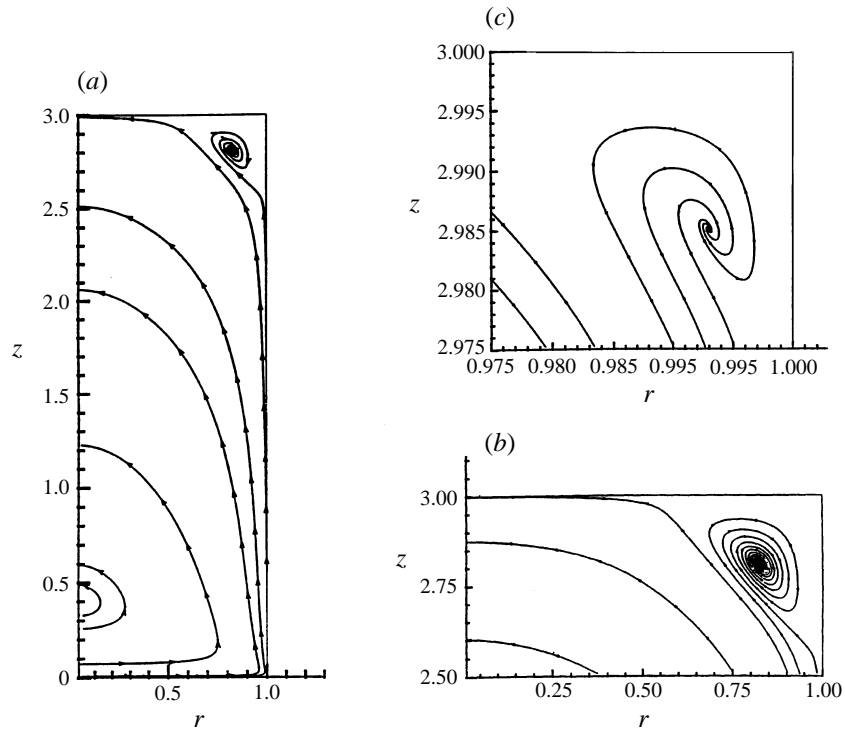


FIGURE 12. (a) Streamlines in the symmetry plane for Stokes flow in a container of height 3. Note that only half the plane is shown. The details of the first corner eddy are shown in (b) while those of the second corner eddy are shown in (c).

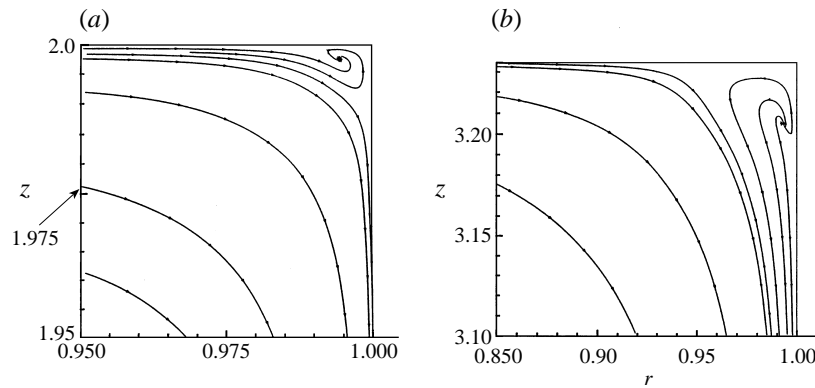


FIGURE 13. Details of the second corner eddies in the plane  $\theta = 0$ . (a)  $h = 2.0$ , (b)  $h = 3.235$ .

corner eddy with height soon after  $h = 3$ . When  $h = 3.1$  the streamlines converging to the focus shown in figure 14(a) have come from the focus at  $\theta = \pi$ ; the width of the eddy on the top of the container is about 0.54. With only a slight increase in height, i.e. when  $h = 3.15$ , the field is significantly different. Streamlines from the other focus continue to stream into this focus, but now instead of converging to the focus they converge to a limit surface  $S_1$ ; meanwhile, streamlines now leave the focus and converge from the inside to  $S_1$  in the same direction as the external streamlines. Note that in figure 14(b) the outgoing streamline has been terminated, for picture clarity,

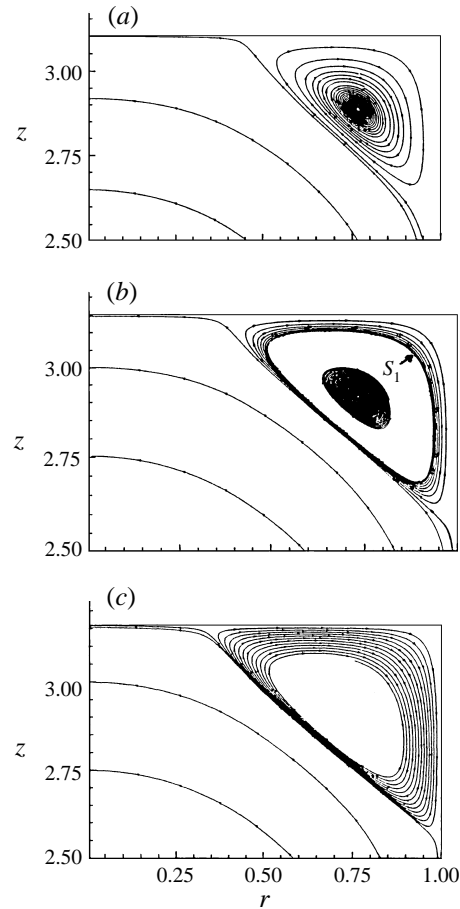


FIGURE 14. Growth and evolution of the first corner eddy, with increasing height, up to first contact in the plane  $\theta = 0$  with  $2.5 \leq z \leq h$ . Note that only the first corner eddies are shown. (a)  $h = 3.1$ , (b)  $h = 3.15$ , (c)  $h = 3.161$ .

before it reaches the limit surface. This intriguing behaviour must have started at a smaller height with the limiting surface growing with  $h$  in a smooth manner.† The need for this will become clear soon enough. Figure 14(c) shows that by the time  $h$  is 3.161,  $S_1$  has grown sufficiently to enable first contact to take place; now, all the streamlines from the focus shown stream into the other focus through a narrow passage adjacent to the lid and the limit surfaces are no longer there. We can now see why the limit surface behaviour soon after  $h = 3.1$  is necessary. If this had not occurred, it is clear from figure 14(a) that at first contact the streamlines on either side of  $r = 0$  would produce a streamline in the main eddy and a streamline from the left focus to the right focus, i.e. it would appear in the wrong direction. These difficulties are avoided by the actually observed behaviour.

† A referee commented “It is possible that the eddy-evolution mechanism discussed in §5 involves a Hopf bifurcation: at a critical value  $h_c$  of the height  $h$ , the stable focus at the first corner eddy evolves into an unstable focus, via the formation of a stable limit cycle (‘limit surface’). These are the characteristics of a Hopf bifurcation. It is interesting that the behaviour local to the eddy depends so crucially on the ‘global’ parameter  $h$ ”. The referee further made the intriguing speculation that  $h_c$  may equal  $\pi$ . Unfortunately, computations show that it is less than  $\pi$ .



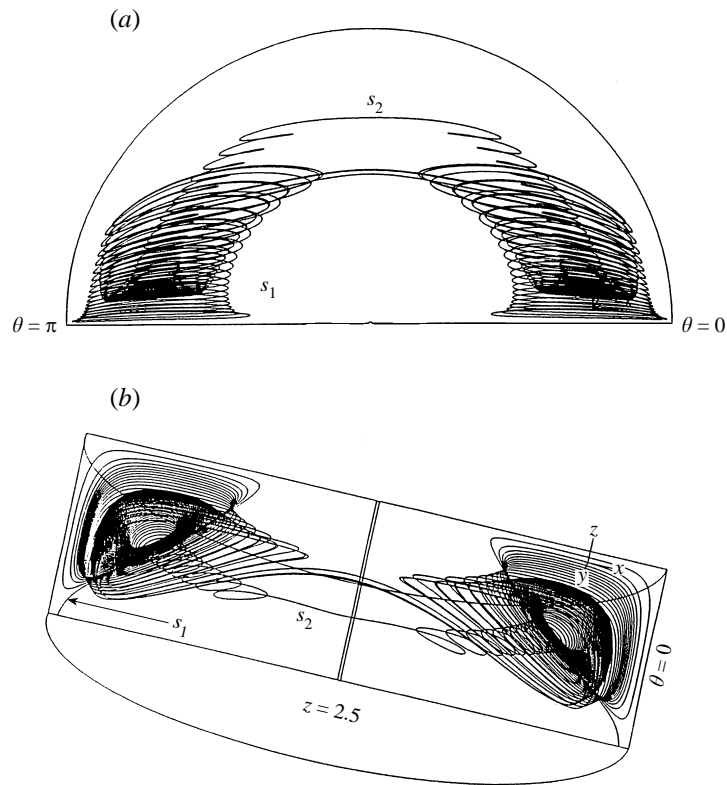


FIGURE 15. Three-dimensional streamlines in the corner eddy region for a container of height 3.15. The same two streamlines  $s_1$  and  $s_2$  are shown in both views of which (a) is in plan looking down on  $z = h$ .

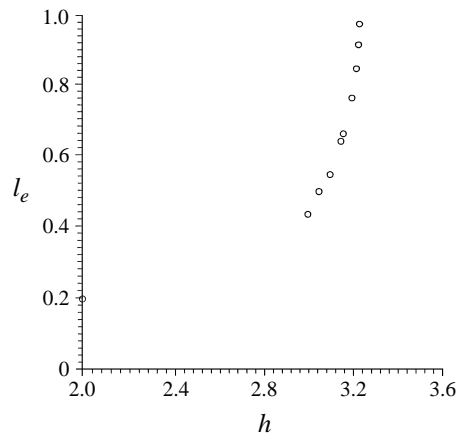


FIGURE 16. The growth of the corner eddy as a function of container height.  $l_e$  is the width of the eddy, up to the point where the radial shear stress vanishes, at the top of the container in the plane  $\theta = 0$ .

A natural question that arises is the behaviour of the flow away from the plane  $\theta = 0$  when a limit surface is present in the corner eddy. Is it really a surface as stated? Figure 15 seems to provide an answer in the affirmative:  $s_1$  is a (closed) streamline that comes from below on the right, makes a number of swirling clockwise loops about the core of the corner eddy, crosses over to the other side, makes an equal number of clockwise

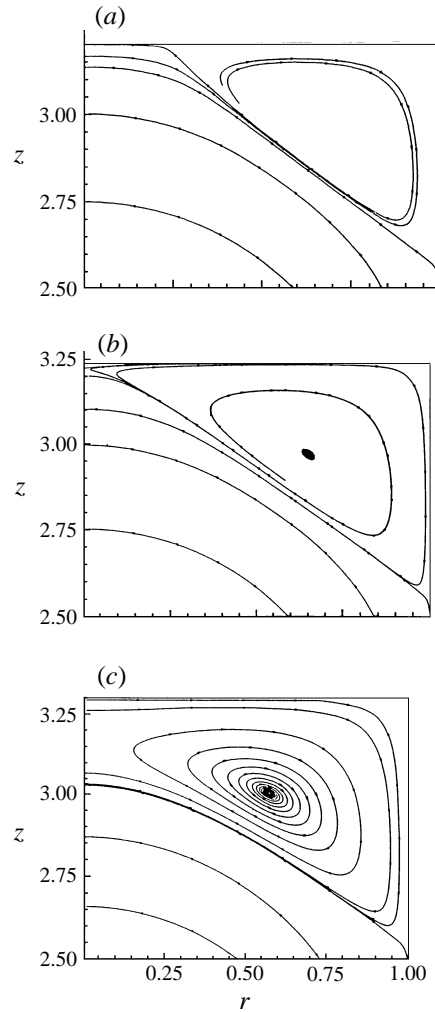


FIGURE 17. Further evolution of the corner eddy after first contact.  
 (a)  $h = 3.2$ , (b)  $h = 3.235$ , (c)  $h = 3.3$ .

loops and then goes on down to the bottom of the container. On the other hand,  $s_2$  is a closed streamline that is confined entirely to the core region of the eddy at the top of the container and generates horn-like surfaces, the outer parts of the horns being bent back. If we examine figure 15(b), starting from the top of the horn close to the plane  $\theta = 0$ , we see that  $s_2$  moves clockwise around the core and around its inner loop, moving outwards to the limit surface  $S_1$  (not shown), which separates it from  $s_1$ . Then, in the company of  $s_1$ , it crosses over to the other side and makes a number of swirling clockwise loops before falling inwards towards the core; now loops of smaller radii are made as  $\theta$  decreases, then it crosses back over to the other side, makes more loops on the smaller radii, before expanding out to the outer horn. These streamline plots tie in nicely with the impression that figure 14 gives of the conditions on the plane of symmetry; together they show how far three-dimensional corner flows differ from their two-dimensional counterparts. Finally, we observe that figure 15 implies the interesting fact that there are two counterflowing azimuthal flows in the core of the eddy; looking in plan, the inner flow is clockwise while the outer flow is anticlockwise.

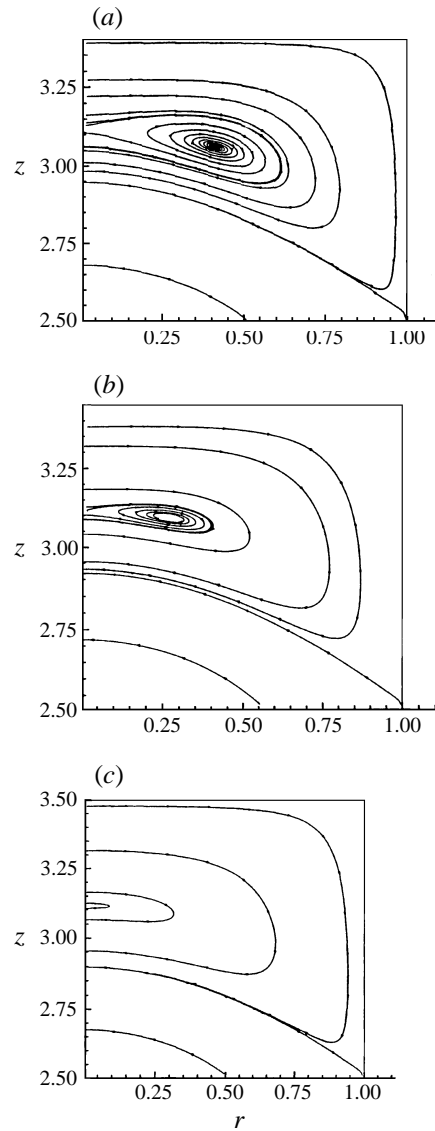


FIGURE 18. Final stages of transition of the first corner eddy into the second primary eddy.  
 (a)  $h = 3.4$ , (b)  $h = 3.45$ , (c)  $h = 3.5$ .

It may have been noted from figure 14 that not only is the ultimate growth of the eddy to first contact very rapid but also that this occurs with very little change in overall eddy size. Let us define  $1 - l_e$  to be the radius at the top of the container where the radial velocity just changes sign off the container; it is the position where the radial shear stress vanishes. Figure 16 shows how  $l_e$ , a measure of the width of the eddy in the plane  $\theta = 0$  along the top of the container, changes with container height. Interestingly, even at first contact, i.e. when  $h \simeq 3.151$ ,  $l_e$  is only about 0.655 as can be seen from figures 14 and 16.

The next stages of the merger process, soon after first contact, are shown in figure 17. When  $h = 3.2$  the flow field is similar to that at  $h = 3.161$  but now  $l_e$  has increased to about 0.756; this is accompanied by a general lifting-off or thickening of the merged

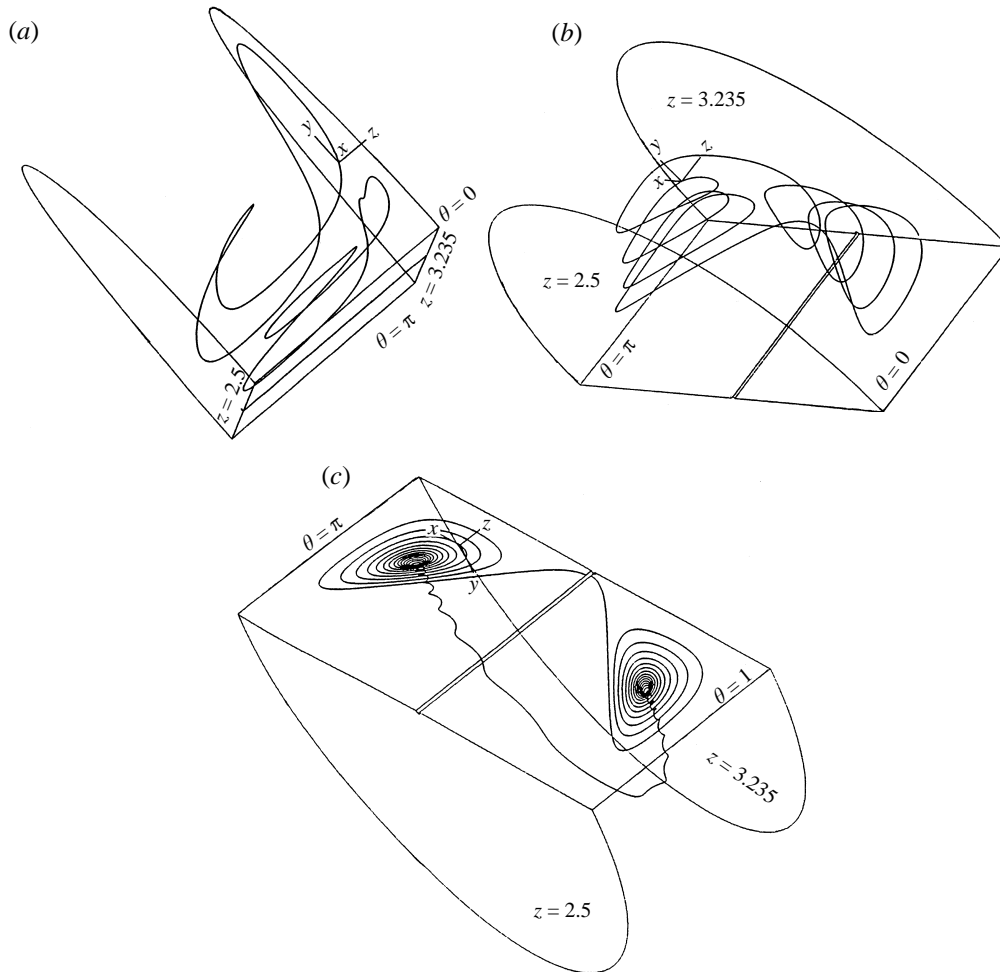


FIGURE 19. Three-dimensional streamline patterns in the merged eddy region,  $h = 3.235$ . (a) Outer streamlines, (b) a streamline which swirls about the core flow, (c) the three-dimensional cat's eye.

portion of the eddy near  $r = 0$ . By the time  $h$  increases to 3.235 the merger is almost complete with  $l_e$  virtually equal to 1. This can be seen in figure 17(b), where there are streamlines from the focus that turn through sharp angles close to  $r = 0$ . The net result of the completion of merger is that the merged eddy is now surrounded by streamlines that do not pass through either focus. This can be clearly seen in figure 17(c) which shows two streamlines enclosing the merged eddies. It is these streamlines which will form the second primary eddy.

It should be noted how different this scenario is from that found in two-dimensional eddy merger (Shankar 1993, figure 7). In that case first contact and final merger took place at the same time since there was no limit surface to contend with. The eddies consisted of closed streamlines with no flow from one side to the other throughout the merger process. It is somewhat surprising that three-dimensional effects are sufficiently significant even in the plane of symmetry that qualitatively new effects are seen.

The final stages of eddy merger and the birth of the second primary eddy are shown in figure 18. When  $h = 3.4$ , the merged eddy has now completely lifted off from the top of the container and the second primary is now fully developed. The merged eddy now

shrinks rapidly as seen in figure 18(b) and by the time  $h = 3.5$  has completely disappeared. Although this figure does not show them, the second corner eddy now takes on the role of the first, growing slowly at first and then, near a critical height, very rapidly until merger leads to the formation of the third primary, and so on. This establishes, in a certain sense, that as in the two-dimensional case the infinite number of corner eddies are the progenitors of the primary eddies.

We conclude by presenting some details of the flow in the merged eddy region for a container of height 3.235, very close to complete merger. Figure 19 shows three sets of three-dimensional streamline patterns. In (a) we see two closed streamlines that do not loop the azimuthal core of the eddy. Their upward movement near  $\theta = \pi/2$  is to accommodate the streamlines from the primary eddy (not shown) that penetrate this region from below. The single streamline in figure 19(b) makes swirling closed loops about the core of the eddy. The upward motion near  $\theta = \pi/2$  is again to accommodate the primary eddy. The streamline in figure 19(c) displays what may be called three-dimensional cat's eyes. Starting from close to the core near the plane  $\theta = 0$ , a particle on this streamline would swirl outwards, almost remaining in a plane, then move over to the other side (near  $\theta = \pi$ ) and swirl inwards to the core. Near the core the swirl is into and along the azimuth until, near  $\theta = 0$ , the swirl is outwards to the starting point. Taken together (a), (b) and (c) give some idea of the complexity of the motion in the merged eddy.

There are a number of features of the streamlines seen here, such as foci, limit lines, 'attractors' etc, which are very reminiscent of certain features often encountered in discussions of nonlinear systems. Here, however, the features are seen in physical space rather than in phase space!

## 6. Conclusion

An eigenfunction expansion method was presented to compute Stokes flow in a cylindrical container driven by the motion of one of the endwalls. The method was used to demonstrate a number of special features of the complex three-dimensional flow field in the container. These included the structure of the main eddy system, the nature of the corner eddies in the symmetry plane, the azimuthal flow away from it and finally the nature of the corner eddy merger leading to the formation of a new primary eddy.

It should perhaps be pointed out that it would be very hard to get as reliable results for this problem by other methods such as by direct numerical computation. This would be especially true for the deeper cavities where the field decays rapidly and which would present severe storage problems. An advantage of the present method is its speed: computations can be carried out for different depths very rapidly. It was this feature that was used to advantage in examining the details of corner eddy merger.

I would like to acknowledge: (i) SERC at the Indian Institute of Science for providing the computational facilities used for this study, (ii) CMMACS at the National Aerospace Laboratories for the use of the 3D graphics used for generating the streamline plots and (iii) AR & DB for financial support through grant number 782. I would also like to thank my colleagues in the Mechanical Engineering Department of the Indian Institute of Science, Bangalore for providing a pleasant environment during my sabbatical, during which period this work was done. Thanks too to Dr Anand Kumar of CMMACS for help in generating the streamline plots and to Dr R. Srinivasan of the Director's Unit for useful discussions. Finally, I would like to acknowledge the useful suggestions made by the referees.

## REFERENCES

- DESHPANDE, M. D. & SHANKAR, P. N. 1994 Direct numerical simulation of a complex turbulent flow. *Current Sci.* **66**, 767.
- DOUGALL, J. 1913 An analytical theory of the equilibrium of an isotropic elastic rod of circular section. *Trans. R. Soc. Edin.* **XLIX**, 895.
- IWATSU R., ISHII, K., KAWAMURA, T., KUWAHARA, K. & HYUN, J. M. 1989 Simulation of transition to turbulence in a cubic cavity. *AIAA Paper* 89-0040.
- MOFFATT, H. K. 1964 Viscous and resistive eddies near a sharp corner. *J. Fluid Mech.* **18**, 1.
- MORSE, P. M. & FESHBACH, H. 1953 *Methods of Theoretical Physics*, Part 2. McGraw-Hill.
- SHANKAR, P. N. 1993 The eddy structure in Stokes flow in a cavity. *J. Fluid Mech.* **250**, 371.
- SHANKAR, P. N. 1996 The real & complex eigenvalues for three-dimensional Stokes flow in a cylindrical container. *NAL Rep.* CF 96 10.
- SRINIVASAN, R. 1995 Accurate solutions for steady plane flow in a driven cavity. I. Stokes flow. *Z. Angew. Math. Phys.* **46**, 524.
- TRAN-CONG, T. & BLAKE, J. R. 1982 General solution of the Stokes' flow equations. *J. Math. Anal. Appl.* **90**, 72.
- VERSTAPPEN, R. W. C. P. & VELDMAN, A. E. P. 1994 Direct numerical simulation of a 3D turbulent flow in a cavity. In *Computational Fluid Dynamics '94* (ed. E. Wagner *et al.*). John Wiley.
- ZANG, Y., STREET, R. L. & KOSEFF, J. R. 1994 A non-staggered grid, fractional step method for time-dependent incompressible Navier–Stokes equations in curvilinear coordinates. *J. Comput. Phys.* **114**, 18.